Transition State Structure for ADP-Ribosylation of Eukaryotic Elongation Factor 2 Catalyzed by Diphtheria Toxin

Sapan L. Parikh and Vern L. Schramm*

Department of Biochemistry, Albert Einstein College of Medicine, Bronx, New York 10461

Received October 27, 2003; Revised Manuscript Received December 4, 2003

ABSTRACT: Bacterial protein toxins are the most powerful human poisons known, exhibiting an LD_{50} of 0.1−1 ng kg^{-1}. A major subset of such toxins is the NAD^+-dependent ADP-ribosylating exotoxins, which include pertussis, cholera, and diphtheria toxin. Diphtheria toxin catalyzes the ADP ribosylation of the diphthamide residue of eukaryotic elongation factor 2 (eEF-2). The transition state of ADP ribosylation catalyzed by diphtheria toxin has been characterized by measuring a family of kinetic isotope effects using ^{3}H-, ^{14}C-, and ^{15}N-labeled NAD^+ with purified yeast eEF-2. Isotope trapping experiments yield a commitment to catalysis of 0.24 at saturating eEF-2 concentrations, resulting in suppression of the intrinsic isotope effects. Following correction for the commitment factor, intrinsic primary kinetic isotope effects of 1.055 ± 0.003 and 1.022 ± 0.004 were observed for [$1_N'$-^{14}C]- and [1_N-^{15}N]NAD^+, respectively; the double primary isotope effect was 1.066 ± 0.004 for [$1_N'$-^{14}C, 1_N-^{15}N]NAD^+. Secondary kinetic isotope effects of 1.194 ± 0.002, 1.101 ± 0.003, 1.013 ± 0.005, and 0.988 ± 0.002 were determined for [$1_N'$-^{3}H]-, [$2_N'$-^{3}H]-, [$4_N'$-^{3}H]-, and [$5_N'$-^{3}H]NAD^+, respectively. The transition state structure was modeled using density functional theory (B1LYP/6-31+G**) as implemented in Gaussian 98, and theoretical kinetic isotope effects were subsequently calculated using Isoeff 98. Constraints were varied in a systematic manner until the calculated kinetic isotope effects matched the intrinsic isotope effects. The transition state model most consistent with the intrinsic isotope effects is characterized by the substantial loss in bond order of the nicotinamide leaving group (bond order = 0.18, 1.99 Å) and weak participation of the attacking imidazole nucleophile (bond order = 0.03, 2.58 Å). The transition state structure imparts strong oxacarbenium ion character to the ribose ring even though significant bond order remains to the nicotinamide leaving group. The transition state model presented here is asymmetric and consistent with a dissociative S_N1 type mechanism in which attack of the diphthamide nucleophile lags behind departure of the nicotinamide.

ADP ribosylation of eukaryotic target proteins is a major biochemical mechanism exploited by bacterial exotoxins to damage human tissues (*1*). The exotoxins disrupt the host by altering intracellular signaling, DNA repair, and cell division (*2*). Cholera and pertussis exotoxins are known to ADP[1] ribosylate G-proteins at specific arginine and cysteine residues and thereby modify signal transduction by G-protein-coupled receptors (*3*, *4*). Diphtheria toxin and *Pseudomonas* exotoxin A ADP ribosylate the sole diphthamide residue of eEF-2. This covalent modification reduces the action of eEF-2 in protein synthesis and results in cell death (*5*).

Diphtheria toxin is one of the three most poisonous substances, comparable to botulism and tetanus toxins. These toxins exhibit LD_{50} values in humans in the range of 0.1−1 ng kg^{-1} (*6*). Produced by the *tox* gene in *Corynebacterium diphtheriae*, diphtheria toxin is synthesized as a single polypeptide chain of 535 amino acids. Selective proteolysis and reduction of a disulfide bond divide the protein into two functionally distinct moieties. Fragment B (37 kDa) is necessary for binding to surface receptors and penetration into cells. Fragment A (21 kDa) catalyzes transfer of the ADP ribosyl group of NAD^+ to the posttranslationally modified histidine residue, diphthamide, of eEF-2 (Figure 1). The covalent modification inactivates eEF-2, disrupting protein biosynthesis and eventually killing the targeted cell. Elongation factor-2 mediates the translocation step in peptide chain elongation by promoting transfer of peptidyl tRNA from the A- to the P-site of the ribosome. The 95 kDa protein is composed of two domains: the N-terminal G-domain responsible for GTP hydrolysis and the C-terminal R-domain, which is hypothesized to interact with the ribosome (*7*). The latter domain contains the posttranslationally modified histidine residue, diphthamide, which requires participation of six genes that can only be found in eukaryotes and archaebacteria (*8*, *9*) (Figure 2). Early kinetic analysis for ADP ribosylation of eEF-2 by diphtheria toxin suggests that the reaction proceeds via an ordered mechanism, the sequence of binding NAD^+ followed by eEF-2 (*10*). In the absence

* To whom correspondence should be addressed. Tel: 718-430-2813. Fax: 718-430-8565. E-mail: vern@aecom.yu.edu.

[1] Abbreviations: eEF-2, eukaryotic elongation factor 2; DTA, catalytic domain of diphtheria toxin; KIEs, kinetic isotope effects; NAD^+, β-nicotinamide adenine dinucleotide; NADH, β-nicotinamide adenine dinucleotide (reduced form); NADPH, β-nicotinamide adenine dinucleotide phosphate (reduced form); $NADP^+$, β-nicotinamide adenine dinucleotide phosphate; ADP, adenosine 5′-diphosphate; ATP, adenosine 5′-triphosphate; AMP, adenosine 5′-monophosphate; GTP, guanosine 5′-triphosphate; PEP, phospho(enol)pyruvate; DTT, dithiothreitol; TCA, trichloroacetic acid; SDS−PAGE, sodium dodecyl sulphate polyacrylamide gel electrophoresis; SDS, sodium dodecyl sulphate; EDTA, ethylenediaminetetraacetic acid; TLC, thin-layer chromatography.

10.1021/bi035907z CCC: $27.50
Published on Web 01/16/2004

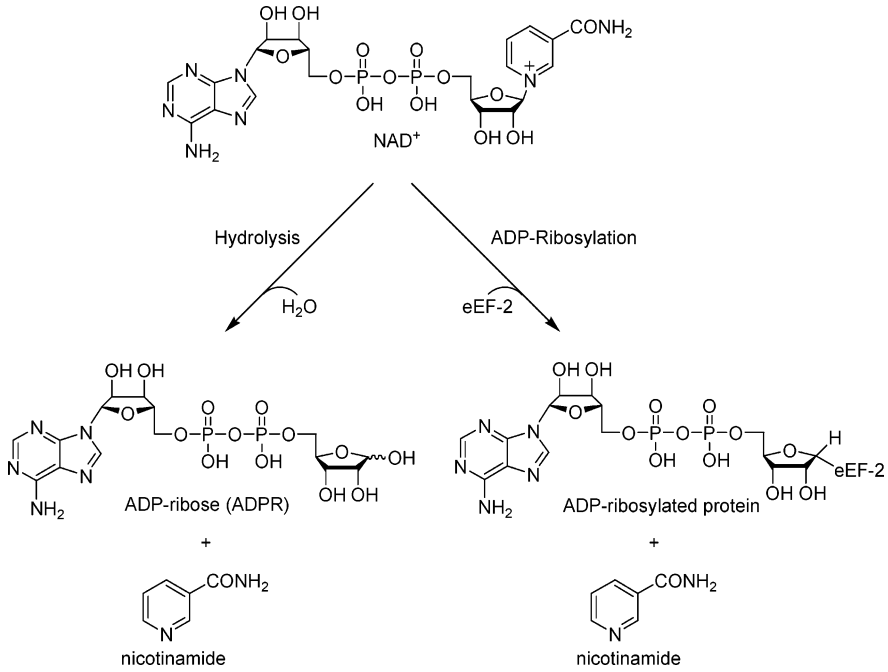

FIGURE 1: NAD^+ hydrolysis and ADP ribosylation of eEF-2 catalyzed by diphtheria toxin.

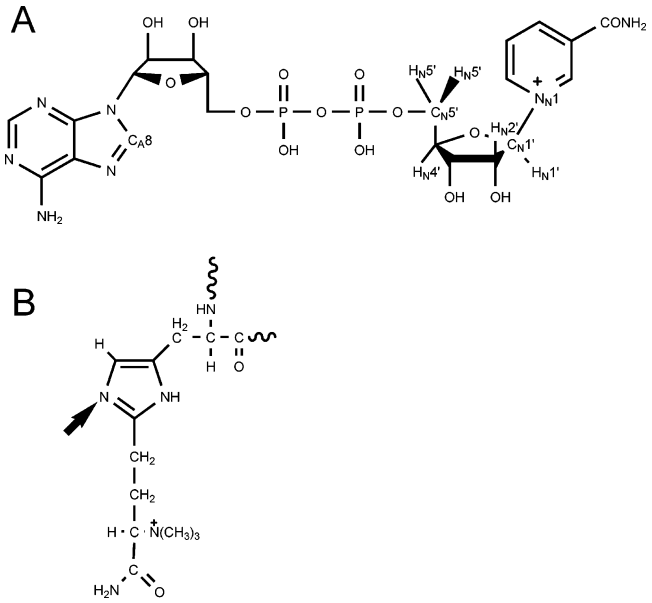

FIGURE 2: (A) Structure of NAD^+. Each numbered position in the molecule was labeled with ^3H, ^{14}C, or ^{15}N for KIEs. The subscript N refers to the NMN^+ portion of the molecule, and subscript A refers to the adenylate portion of the molecule. (B) Diphthamide, the modified histidine ADP ribosylated by diphtheria toxin. The site of ADP ribosylation is indicated with an arrow. In yeast eEF-2, this position is His699.

of eEF-2, diphtheria toxin catalyzes the slow hydrolysis of NAD^+ at the C1′−N1 glycosyl bond to form ADP ribose and nicotinamide. This hydrolytic reaction is not thought to have biological significance, since the hydrolytic rate is only 1/1700 that of the k_{cat} for ADP ribosylation of eEF-2 (Figure 1) (*11*).

Bacterial ADP ribosyltransferases have been well-studied since clinically important pathogenic bacterial diseases, including diphtheria, cholera, and pertussis, damage human tissue by the action of these toxins. Blocking the action of the toxins prevents the disease; thus, the antigen used to prevent diphtheria is inactivated diphtheria toxin. With incomplete vaccination programs, there is a critical need for the development of novel therapeutics that are effective against these diseases. Blocking the action of exotoxins places no selective pressure on the bacteria; thus, antibiotics against antitoxins are not expected to induce resistance. Knowledge of enzymatic transition states is highly predictive for design of transition state analogues. Specific inhibitors against bacterial exotoxins have the potential to form a permanent addition to antibacterial antibiotics.

Earlier studies reported that ADP ribosylation of $G_{s\alpha}$, $G_{i\alpha}$, and eEF-2 proteins catalyzed by cholera, pertussis, and diphtheria toxin, respectively, occurs via inversion of configuration at the C1′-carbon of the ribose ring (*12*−*14*). Products resulting from the ADP ribosyltransferase reaction with the appropriate nucleophile all exhibited the α-configuration at C1′ of ADP ribose. As part of our efforts to develop transition state analogues, we have characterized the transition state for the ADP ribosylation of eEF-2 by diphtheria toxin using competitive KIEs, substrate partitioning, and computational chemistry methods. The results permit the determination of intrinsic isotope effects, which are used to illustrate a geometric model of the enzymatic transition state. The transition state structure and stereochemical configuration provide a blueprint for the design of transition state inhibitors for diphtheria toxin.

MATERIALS AND METHODS

Materials. ^3H- and ^{14}C-labeled glucose and ^{14}C-labeled ATP were purchased from American Radiolabeled Chemicals, Inc. and were used without further purification. β-NAD^+, $NADP^+$, NADPH, ATP, ADP, PEP, pyruvate, glutamic acid, α-ketoglaturic acid, nicotinic acid, and all other biochemicals and enzymes for NAD^+ synthesis were purchased from Sigma Chemical Company. All chromatography solvents, bacterial growth and expression media, and buffer salts were from Fisher Scientific.

NAD^+ isotopically labeled at specific sites was prepared enzymatically from ^3H-, ^{14}C-, and ^{15}N-labeled glucose,

ribose-5-phosphate, ATP, and nicotinic acid, according to published procedures (*15*). Labeled NAD^+ was purified by C18 reverse phase high-performance liquid chromatography (HPLC) with 100 mM ammonium acetate, pH 5.0, containing 2% methanol. The isotopically labeled substrates prepared for these studies are listed in Table 2, and the nomenclature for the labels is depicted in Figure 2. A pPROEX prokaryotic expression plasmid containing the His-6 tagged gene for NAD^+ pyrophosphorylase (hs-PNAT3) was a kind gift from Professor Hong Zhang, University of Texas Southwestern Medical Center, and was expressed and purified to homogeneity following the procedures described by Zhang et al. (*16*). NadE from *C. glutamicum* and *H. pylori* was a generous gift from Dr. Konstantin Shatalin, Intergrated Genomics Inc. The *E. coli* strain BL21(DE3) containing the His-6 tagged gene of the DTA was a kind gift from Professor R. John Collier at Harvard Medical School. DTA was expressed and purified as described by the methods of Wilson et al. (*17*). eEF-2 was isolated and purified from type I Bakers yeast as previously described (*18*). The identity of the 95 kDa protein was confirmed by N-terminal sequence analysis. The purity of the proteins was verified by SDS−PAGE and was determined to be >98%. Protein concentration was determined at 595 nm according to Bradford methods (*19*). All proteins were dispensed into small aliquots and frozen at −80 °C for storage and thawed prior to use.

NAD^+ Glycohydrolase Assay. The NAD^+ glycohydrolase activity of DTA was determined by following the release of labeled nicotinamide from [*carbonyl*-^{14}C]NAD^+. The assay was conducted over 6 h at 37 °C in a final volume of 100 μL containing 100 mM Tris-HCl (pH 8.0), 1 mM EDTA, 20 mM DTT, 2−10 μM [*carbonyl*-^{14}C]NAD^+, and 7.25 μM DTA. Aliquots at 15, 30, 45, 60, 120, 240, and 360 min were applied to DEAE cellulose TLC plates and developed in 70/30 (95% ethanol/1 M ammonium acetate, pH 7.5). The hydrolyzed [*carbonyl*-^{14}C]nicotinamide and [*carbonyl*-^{14}C]-NAD^+ were separated and quantitated by liquid scintillation counting. Kinetic parameters, k_{cat} and K_m, were obtained by fitting initial reaction rate data to the Michaelis−Menten equation, using Kaleidagraph (version 3.52).

ADP Ribosyltransferase Assay. Initial rates for the ADP ribosyltransferase reaction catalyzed by diphtheria toxin were determined by measuring the extent of incorporation of radioactivity from [^{32}P]NAD^+ into TCA precipitable material using purified eEF-2 as the ADP ribose acceptor. The standard kinetic assay consisted of a 200 μL reaction mixture of 100 mM Tris-HCl (pH 8.0), 1 mM EDTA, 20 mM DTT, and 0.8 nM of diphtheria toxin. k_{cat} and K_m for eEF-2 were determined at a fixed, saturating concentration of NAD^+ (825 μM) and by varying the concentration of eEF-2 (0.5−25 μM). k_{cat} and K_m for NAD^+ were determined at a fixed, saturating concentration of eEF-2 (10 μM) and by varying the concentration of NAD^+ (1−100 μM). The reaction was started by adding NAD^+ (0−1 mM NAD^+) and 200 000 cpm of [^{32}P]NAD^+. Aliquots (30 μL) were removed at 0, 1, 2, 3, 4, and 5 min and pipetted into 50 μL of 5 mM unlabeled NAD^+ and precipitated by adding 80 μL of 30% TCA. The precipitate was washed twice with 500 μL of 5% TCA solution, followed by 500 μL of acetone and dissolved in 1 mL of 10% SDS in 200 mM Tris-HCl, pH 8.0. The sample was mixed with 10 mL of scintillation fluid and analyzed by scintillation counting to quantitate radioactivity in the ADP-ribosylated product. The kinetic parameters for ADP ribosyltransferase activity were analyzed by fitting data to the Michaelis−Menten equation from assays preformed in triplicate in at least three independent experiments.

Commitment to Catalysis. Isotope trapping experiments were carried out using pulse−chase methods outlined by Rose (*20*, *21*). A 10 μL reaction mixture containing 50 μM DTA and 200 μM NAD^+ including 500 000 cpm [^{32}P]NAD^+ was incubated at 25 °C for 15 s. The sample was diluted with 100 μL of 40 mM unlabeled NAD^+ containing variable concentrations of eEF-2. The sample was incubated at 37 °C to allow 10 catalytic turnovers and terminated by the addition of 110 μL of 30% TCA solution. The precipitate was washed twice with 500 μL of 5% TCA solution, followed by 500 μL of acetone and dissolved in 1 mL of 10% SDS in 200 mM Tris-HCl, pH 8.0. The sample was mixed with 10 mL of scintillation fluid and analyzed by scintillation counting to quantitate the ADP-ribosylated product. In control experiments for the formation of ADP-ribosylated protein during the incubation step, reaction mixtures containing identical amounts of DTA, [^{32}P]NAD^+, unlabeled NAD^+, and eEF-2 were incubated for the same length of time. The labeled ADP-ribosylated protein was treated as described above.

KIEs. KIEs for ADP ribosylation were determined by competitive methods using radiolabeled NAD^+ (*22*). Radiolabeled NAD^+ was incubated with DTA and eEF-2 as the limiting reagent. A reaction mixture containing 150 000 cpm of ^{3}H and 50 000 cpm ^{14}C of each isotope in a sensitive and a remote position was adjusted with unlabeled NAD^+ to give a final concentration of 40 μM. The mixtures were purified on C18 reverse phase HPLC in 100 mM ammonium acetate, pH 5.0, containing 2% methanol and lyophilized. For each KIE experiment, two identical reaction mixtures were analyzed, both using the same substrate mixture. One was allowed to react to 25% conversion and the other to 100% completion. The 100 μL reaction mixture contained 1 μM DTA and 10 μM eEF-2 for the 25% conversion and 2.7 μM DTA and 20 μM eEF-2 for the 100% conversion. The reactions were started by the addition of NAD^+, and the samples were incubated for 4 h in 100 mM Tris-HCl (pH 8.0), 1 mM EDTA, and 20 mM DTT at 37 °C. Aliquots of 30 μL were added to 70 μL of stop solution containing 10 mM unlabeled NAD^+ and precipitated with 100 μL of 30% TCA. The precipitate was washed twice with 500 μL of 5% TCA solution, followed by 500 μL of acetone and dissolved in 1 mL of 10% SDS in 200 mM Tris-HCl, pH 8.0. The ^{3}H/^{14}C ratio for the partial and complete conversions was measured by scintillation counting. The samples were analyzed for 10 counting cycles of 10 min per sample. The observed KIEs are determined from the ^{3}H/^{14}C ratio for the partial reaction, and the complete reaction is fitted to the equation below where f is the fraction of NAD^+ converted to ADP-ribosylated eEF-2 and the $KIE_{observed}$ is the experimental value for the KIE.

$$\text{corrected KIE} = \ln (1 - \text{KIE}_{\text{observed}} f)/\ln (1 - f)$$

Transition State Modeling. Transition state structure optimization, energy, and frequency calculations for the ADP ribosyltransferase reaction catalyzed by diphtheria toxin were preformed using the Gaussian 98 suite of programs (*23*),

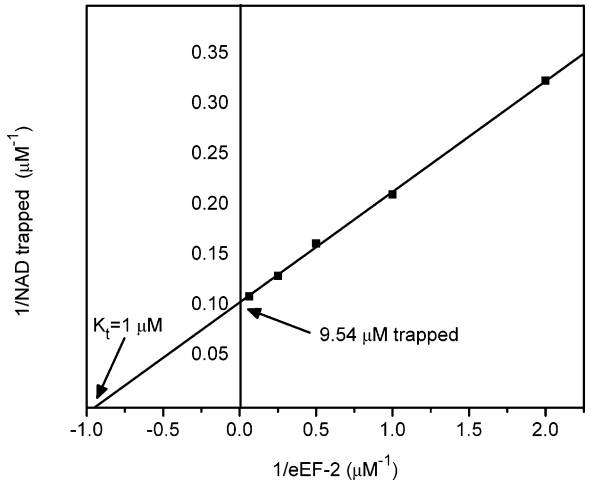

FIGURE 3: Commitment to catalysis for the ADP ribosylation of eEF-2 by DTA. The pulse portion of the experiment contained 50 μM DTA and 200 μM NAD$^+$ including 500 000 cpm [^{32}P]NAD$^+$ in 100 mM Tris-HCl (pH 8.0), 1 mM EDTA, and 20 mM DTT. The chase solution contained 40 mM NAD$^+$, and the concentration of eEF-2 varied from 0.5 to 16 μM. The intercept value indicates that 9.54 μM ADP-ribosylated eEF-2 was formed from 50 μM DTA−[^{32}P]NAD$^+$ complex.

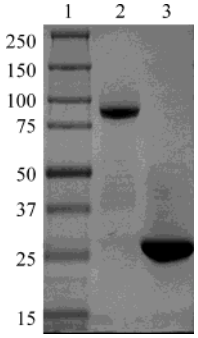

FIGURE 4: SDS−PAGE of purified DTA and eEF-2. Lane 1, molecular weight maker; lane 2, eEF-2; and lane 3, DTA.

using the density functional level of theory (B1LYP/6-31+G**). Atomic coordinates for the reactant state for the NMN$^+$ portion of NAD$^+$ were derived from the crystal structure of NAD$^+$ bound to diphtheria toxin (*24*). Hydrogen atoms were placed in their energetic minima, and the nicotinamide ribonucleoside portion of NAD$^+$ was optimized by the density functional level of theory. Three dihedral angles within the ribose ring were constrained during the reactant state minimization to maintain the 3′-endo conformation reported in the crystal structure ($O_4-C_4-C_3-C_2$ at −20.9°, $C_1-C_2-C_3-C_4$ at −27.2°, and $C_4-O_4-C_1-C_2$ at 11.7°). The incoming nucleophile (the ring nitrogen of diphthamide) was modeled as an attacking imidazole in the transition state search models. The transition state model whose calculated KIEs matched the experimentally derived intrinsic KIEs was located by systematically varying C1′−N1, C1′−nucleophile, C1′−O4′, C1′−C2′, C1′−H1′, and C2′−H2′ bond lengths and related bond angles and dihedral angles while allowing the rest of the molecule to be optimized as described above (Figure 5). The transition state structure included one imaginary frequency, corresponding to the transition from reactants to products by translation of the N1−C1′ bond. Intrinsic KIEs were calculated from the Gaussian-derived force constants using the Isoeff 98 program (*25*). This approach differs from the earlier method of linear

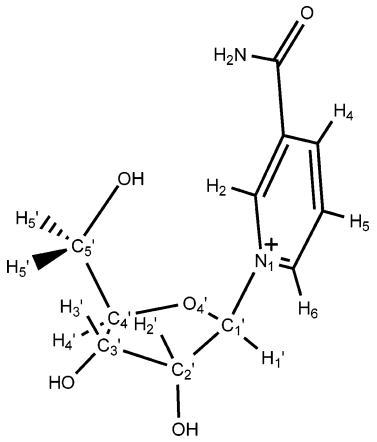

FIGURE 5: Structure of the nicotinamide ribonucleoside portion of NAD$^+$ used in the ab initio analysis for KIEs using Gaussian 98.

extrapolation between force constants for stable bonds as bond order changes (e.g., refs *22* and *26*) and is therefore proposed to provide more accurate models of transition state structure from KIE data.

RESULTS AND DISCUSSION:

Expression and Purification of DTA and Isolation of eEF-2 from Bakers Yeast. DTA was expressed with an N-terminal His-tag sequence to facilitate purification. This enabled the single step purification of the 21 kDa protein using metal affinity chromatography. This method yielded approximately 80 mg of purified protein from 1 L of bacterial culture. The protein purity was greater than 98%, as estimated by SDS−PAGE (Figure 4). eEF-2 was isolated and purified to homogeneity from type 1 bakers yeast. The N terminus of the 95 kDa protein, eEF-2, was verified by Edman degradation. The protein sequence was NH_2-***VAFTVDQ***-COOH. The purity of eEF-2 (>98%) was determined by SDS−PAGE (Figure 4).

NAD$^+$ Glycohydrolase and ADP Ribosylation Activities. Diphtheria toxin catalyzes the slow hydrolysis of NAD$^+$ in the absence of eEF-2, a reaction with no known physiological significance. A k_{cat} of 0.11 ± 0.01 min^{-1}, K_m for NAD$^+$ of 85 ± 13 μM, and k_{cat}/K_m of 0.001 μM^{-1} min^{-1} were determined at 37 °C in 100 mM Tris-HCl, 1 mM EDTA, and 20 mM DTT, pH 8.0. Earlier studies on NAD$^+$ glycohydrolase activity have resulted in K_m values in the range of 11−270 μM and k_{cat} of 0.015−0.180 min^{-1} with variable temperature and/or buffer conditions, including phosphate (*17*, *26*−*28*). Kinetic parameters k_{cat}, K_m, and k_{cat}/K_m for the ADP ribosyltransferase reaction were determined under the same conditions and are summarized in Table 1. A K_m value of 6 ± 2 and 0.65 ± 0.06 μM was found for NAD$^+$ and eEF-2, respectively, for the ADP ribosyltransferase reaction. These numbers are in good agreement with the K_m values of 9 μM for NAD$^+$ and 0.9 μM for eEF-2 reported earlier (*17*). Although diphtheria toxin catalyzes both the hydrolysis of NAD$^+$ and the ADP ribosylation reaction, at 37 °C, the k_{cat} for ADP ribosylation is 182 ± 15 min^{-1}, 1700-fold greater than the rate of hydrolysis, indicating that the hydrolytic reaction does not influence the KIE determination.

Commitment to Catalysis. Isotope trapping experiments outlined by Rose (*20*, *21*) were used to determine commitment factors for ADP ribosylating toxins (*22*, *29*). Commit-

Table 1: Kinetic Constants for the Reaction Catalyzed by Diphtheria Toxin[a]

reaction	$K_{m\ (NAD)}$ (μM)	$K_{m\ (eEF-2)}$ (μM)	k_{cat} (min^{-1})	$k_{cat}/K_{m\ (NAD)}$ ($\mu M^{-1}\ min^{-1}$)	$k_{cat}/K_{m\ (eEF-2)}$ ($\mu M^{-1}\ min^{-1}$)
hydrolysis	85 ± 13		0.11 ± 0.01	0.001	
ADP ribosylation	6 ± 2	0.65 ± 0.06	182 ± 15	30	280

[a] Conditions: 100 mM Tris-HCl, 1 mM EDTA, and 20 mM DTT, pH 8.0, 37 °C.

Table 2: KIEs for the ADP Ribosylation of eEF-2 and Hydrolysis by Diphtheria Toxin

substrate	experimental DTA ADPRT KIE	intrinsic DTA ADPRT KIE[b]	intrinsic DTA hydrolysis KIE[d]
[$1_N'$-^{14}C]- and [$5_N'$-^{3}H]NAD$^+$	1.044 ± 0.003[a]	1.055 ± 0.003 (3)[c]	1.034 ± 0.004
[1_N-^{15}N]- and [$5_N'$-^{3}H]NAD$^+$	1.018 ± 0.004[a]	1.022 ± 0.004 (3)	1.030 ± 0.004
[1_N-^{15}N, $1_N'$-^{14}C]-, and [$5_N'$-^{3}H]NAD$^+$	1.053 ± 0.004[a]	1.066 ± 0.004 (4)	1.062 ± 0.010
[$1_N'$-^{3}H]- and [8_A-^{14}C]NAD$^+$	1.157 ± 0.002	1.194 ± 0.002 (4)	1.200 ± 0.005
[$2_N'$-^{3}H]- and [8_A-^{14}C]NAD$^+$	1.081 ± 0.003	1.101 ± 0.003 (4)	1.142 ± 0.003
[$4_N'$-^{3}H]- and [8_A-^{14}C]NAD$^+$	1.011 ± 0.005	1.013 ± 0.005 (3)	0.990 ± 0.002
[$5_N'$-^{3}H]- and [8_A-^{14}C]NAD$^+$	0.990 ± 0.002	0.988 ± 0.002 (3)	NA
[$5_N'$-^{3}H]- and [$5_N'$-^{14}C]NAD$^+$	0.990 ± 0.004	0.987 ± 0.004 (3)	1.032 ± 0.004

[a] KIE experiments that use [$5_N'$-^{3}H]NAD$^+$ as a remote label are corrected by the formula (observed KIE × [$5_N'$-^{3}H]NAD$^+$ KIE). Conditions: 100 mM Tris−HCl, 1 mM EDTA, and 20 mM DTT, pH 8.0, 37 °C. [b] Intrinsic KIEs were calculated by the formula $(KIE_{ex} - 1)C_f + KIE_{ex} = KIE_{int}$. [c] The number of triplicate sample experiments is shown in parentheses (each KIE reaction mixture was analyzed in triplicate). The KIE values for all individual experimental samples (9−12) were averaged, and the standard error of the experiments was calculated. [d] Hydrolysis of NAD$^+$ catalyzed by DTA was at 37 °C in 50 mM potassium phosphate buffer, pH 6.0. The data were taken from ref *26*.

ment factor in the forward direction was determined by mixing diphtheria toxin with [^{32}P]NAD$^+$ to form the Michaelis complex, followed by a chase solution containing excess unlabeled NAD$^+$ (>200 000-fold) and variable concentrations of eEF-2. A fraction of toxin-bound [^{32}P]NAD$^+$ in the binary complex was converted to [^{32}P]ADP ribosyl eEF-2 as a function of eEF-2 concentration. When extrapolated to saturating eEF-2 concentration, 9.54 μM ADP-ribosylated eEF-2 was formed with diphtheria toxin at 50 μM. Forward commitment for ADP ribosylation is defined by the ratio of NAD$^+$ converted to ADP-ribosylated eEF-2 relative to the NAD$^+$ released. The experimentally measured forward commitment factor was determined to be 0.24 at saturating eEF-2 (Figure 3). Commitment factors and K_t were determined by plotting $1/NAD_{trapped}^+$ (μM^{-1}) vs 1/eEF-2 (μM^{-1}). K_t is the concentration of eEF-2 that causes half-maximal trapping, thus $K_t \approx K_m$ (*20*). The experimental value for K_t was 1 μM and is in good agreement with the K_m value of 0.65 μM. The observed KIEs are corrected for the forward commitment and listed in Table 2.

The effects of forward and reverse commitment factors govern experimentally observed KIEs and are predicted by the equation derived by Northrop (*30*):

$$^3V/K = (^3k + C_f + C_r{}^3K_{eq})/(1 + C_f + C_r)$$

where $^3V/K$ is an observed tritium isotope effect, ^3k is the intrinsic isotope effect on the isotopically sensitive step, C_f and C_r are the forward and reverse commitment factors, respectively, and $^3K_{eq}$ is the equilibrium isotope effect. Because covalent modification of eEF-2 is experimentally irreversible, the reversible commitment is insignificant relative to the others terms in the equation above and reduces the expression to:

$$^3V/K = (^3k + C_f)/(1 + C_f)$$

This experiment reveals the probability that NAD$^+$ bound in the Michaelis complex will be converted to product, relative to being released as unchanged substrate. It has been suggested from kinetic, chemical, and X-ray studies that diphtheria toxin catalyzes an ordered sequential mechanism with NAD$^+$ binding before eEF-2 (*10*, *13*, *24*). The commitment factor of 0.24 for NAD$^+$ at saturating eEF-2 establishes that NAD$^+$ can exchange from the ternary complex. Thus, the mechanism is likely to contain some random character.

KIEs. KIE measurements required the synthesis of ^{3}H, ^{14}C, and ^{15}N labels in an isotopically sensitive position of the NMN$^+$ portion of NAD$^+$ and remote labels in an isotopically insensitive position (Figure 2). The methodology toward the enzymatic synthesis of these compounds was based on published procedures (*15*). The following molecules were synthesized with labels in the sensitive positions: [$1_N'$-^{14}C]-, [1_N-^{15}N]-, [1_N-^{15}N, $1_N'$-^{14}C]-, [1_N-^{15}N, $5_N'$-^{14}C]-, [$1_N'$-^{3}H]-, [$2_N'$-^{3}H]-, [$4_N'$-^{3}H]-, and [$5_N'$-^{3}H]NAD$^+$. Labels in the remote region were [$5_N'$-^{14}C]- and [$8_A'$-^{14}C]NAD$^+$ for measuring ^{3}H KIEs and [$5_N'$-^{3}H]NAD$^+$ for ^{14}C KIEs. Radiolabeled NAD$^+$ was analyzed for purity by HPLC (>99%). The TCA precipitation method was used to analyze the ^{3}H/^{14}C isotopic ratio in ADP-ribosylated protein.

4′-^{3}H and 5′-^{3}H KIEs. The remote KIEs of 1.013 ± 0.005 for [$4_N'$-^{3}H]NAD$^+$ and 0.988 ± 0.002 for [$5_N'$-^{3}H]NAD$^+$ were measured using [$5_N'$-^{14}C]NAD$^+$. To rule out the participation or contribution of a ^{14}C effect at the 5′-carbon of ribose, [$8_A'$-^{14}C]NAD$^+$ was also used as a remote label in separate experiments. The results yielded identical values within experimental error with ^{14}C at [$5_N'$-^{14}C]NAD$^+$ or [$8_A'$-^{14}C]NAD$^+$ (Table 3). The magnitude of these KIEs is characteristic of *N*-ribosyl transferase reactions (*29*, *31*, *32*) and can be attributed to distortion of geometry of the 4′- and 5′-hydrogens at the transition state relative to the geometry when free in solution. Chemical solvolysis studies of NAD$^+$ have resulted in isotope effects of unity at these positions, also indicating that the measured isotope effects must arise from enzyme−NAD$^+$ interaction (*33*).

Table 3: Intrinsic KIEs for the ADP Ribosylation vs Calculated

substrate	sensitive isotopic label	DTA ADPRT KIE[a]	calculated[b]
[1_N′-^{14}C]- and [5_N′-^{3}H]NAD$^+$	^{14}C, primary[a]	1.055 ± 0.003 (3)	1.051
[1_N-^{15}N]- and [5_N′-^{3}H]NAD$^+$	^{15}N, primary[a]	1.022 ± 0.004 (3)	1.017
[1_N-^{15}N, 1_N′-^{14}C]- and [5_N′-^{3}H]NAD$^+$	^{15}N and ^{14}C double primary[a]	1.066 ± 0.004 (4)	1.070
[1_N′-^{3}H]- and [8_A-^{14}C]NAD$^+$	^{3}H, α-secondary	1.194 ± 0.002 (4)	1.196
[2_N′-^{3}H]- and [8_A-^{14}C]NAD$^+$	^{3}H, β-secondary	1.101 ± 0.003 (4)	1.101
[4_N′-^{3}H]- and [8_A-^{14}C]NAD$^+$	^{3}H, γ-secondary	1.013 ± 0.005 (3)	1.021
[5_N′-^{3}H]- and [8_A-^{14}C]NAD$^+$	^{3}H, δ-secondary	0.988 ± 0.002 (3)	0.996
[5_N′-^{3}H]- and [5_N′-^{14}C]NAD$^+$	^{3}H, δ-secondary	0.987 ± 0.004 (3)	0.996

[a] Observed isotope effects were corrected as in the legend to Table 2. Conditions: 100 mM Tris-HCl, 1 mM EDTA, and 20 mM DTT, pH 8.0, 37 °C. [b] Transition state structure optimizations for the ADP ribosylation of eEF-2 catalyzed by diphtheria toxin were preformed using Gaussian 98 at density functional level of theory (B1LYP/6-31+G**).

1′-^{14}C and 1-^{15}N KIEs. A relatively large KIE of 1.055 ± 0.003 was observed for [1_N′-^{14}C]NAD$^+$. The [1′-^{14}C] KIE was larger than that for the NAD$^+$ hydrolysis catalyzed by diphtheria toxin, 1.034 ± 0.004, whereas the [1-^{15}N] isotope effects for both the transferase and hydrolytic reactions were similar within experimental error (*26*). The [1′-^{14}C] KIE for the transfer reaction signifies significant participation of the attacking and/or departing nucleophiles at the transition state, while the small KIE for the hydrolytic reaction indicated weak nucleophilic participation of the attacking and departing nucleophiles (*26*). Studies by Mentch and co-workers on the *N*-riboside hydrolysis of AMP have demonstrated [1′-^{14}C] isotope effects of 1.03−1.05 for C−N bond orders of 0.1−0.4 at the transition state when the attacking water nucleophile was fixed at bond order of 0.03 (*34*). The primary KIE of 1.022 ± 0.004 at [1-^{15}N] is indicative of extensive loss of bond order of the nicotinamide leaving group since the maximum value for this isotope effect is below 1.040. This value is in close agreement with other ADP-ribosylating toxin catalyzing similar chemistry (*22*, *26*, *29*, *35*). The intrinsic double primary, [1_N′-^{14}C, 1_N′-^{15}N], KIE of 1.066 ± 0.004 was found to be within close agreement with the 1.078 ± 0.007 from the product of the single primary KIEs.

1′-^{3}H and 2′-^{3}H KIEs. A relatively large α-secondary [1′-^{3}H] KIE of 1.194 ± 0.002 and a β-secondary [2′-^{3}H] KIE of 1.101 ± 0.003 were observed for the ADP ribosyltransferase reaction. A similar KIE of 1.200 ± 0.005, at [1′-^{3}H], was observed for the hydrolytic reaction. The large α-secondary KIE at [1′-^{3}H] is attributed to significant out of plane bending of the C1′−H1′ bond as C1′ rehybridizes toward sp^2 geometry at the transition state. The large value of the [1′-^{3}H] and [2′-^{3}H] KIEs indicates substantial development of a ribooxocarbenium ion-like transition state with significant sp^2 hybridization at C1′. A larger [2′-^{3}H] KIE for NAD$^+$ hydrolysis by diphtheria toxin, 1.142 ± 0.003, was observed as compared to the transferase reaction, 1.101 ± 0.003. The [2′-^{3}H] KIE results from the hyperconjugation effect observed between the occupied π-orbital of the C2′-carbon and the empty p-orbital of the anomeric C1′-carbon (*34*). This results in a decrease in bond order between C2′−H2′ atoms and is dependent on the dihedral angle between N1−C1′−C2′−H2′ at the transition state. The effect is largest when orbital overlap maximizes at 0 and 180° for this dihedral but also depends on the extent of sp^2 hybridization at C1′. The conformation of the ribose ring at the transition state for ADP ribosylation and NAD$^+$ hydrolysis reactions catalyzed by bacterial toxins has been reported from our previous work and is consistent with a change in ribosyl pucker from 3′-endo in the reactant state to 3′-exo at the transition state (*12*, *22*, *26*, *29*, *35*, *36*). This result is also consistent for the ADP ribosylation of eEF-2 reported here.

Table 4: Bond Order and Bond Length for NAD$^+$ Reactant and Transition State Structures for ADP Ribosylation of eEF-2 and NAD$^+$ Hydrolysis by DTA

			transition state structure for diphtheria toxin			
	reactant structure NAD$^+$[a]		eEF-2−ADP ribosylation		NAD$^+$ hydrolysis	
bond	bond order	Å	bond order	Å	bond order	Å
C1′−N1	0.824	1.533	0.180	1.990	0.020	2.644
C1′−O4	1.062	1.392	1.400	1.309	1.665	1.257
C1′−C2′	0.936	1.546	0.990	1.529	1.073	1.505
C1′−H1′	0.988	1.094	1.051	1.076	1.062	1.072
C2′−H2′	0.983	1.095	0.884	1.127	0.987	1.094
C1′−N_{nuc}	0.001	3.500	0.025	2.580	0.031	2.451

[a] Values for the reactant NMN$^+$ portion of NAD$^+$ were derived from geometry optimization calculated by Gaussian 98. Atomic coordinates were from the crystal structure of NAD$^+$ bound to diphtheria toxin (*24*). [b] Pauling bond order, defined as $n_i = \exp[(r_1 - r_i)/0.3]$ where r_1 is the bond length of a single bond. Single bond lengths were as follows: C−C, 1.526 Å; C−N, 1.475 Å; C−O, 1.41 Å; and C−H, 1.09 Å. [c] Pauling bond order and bond lengths at the transition state structures for ADP ribosylation of eEF-2 and NAD$^+$ hydrolysis, respectively. Values for NAD$^+$ hydrolysis are from ref *26*.

Transition State Structure. The transition state structure for ADP ribosylation of eEF-2 is consistent with significant bond order of 0.18 (1.99 Å) for the *N*-ribosidic bond. By comparison, the slow hydrolysis of NAD$^+$ by DTA has a *N*-ribosidic bond order of 0.02 (2.64 Å) for NAD$^+$ hydrolysis (Table 4). Both ADP ribosyltransferase and NAD$^+$ glycohydrolase reactions indicate weak participation of the water or imidazole nucleophiles with a bond order ∼0.03. Reaching the transition state with a bond order of 0.18 to the leaving group establishes that DTA catalyzes the reaction with an earlier transition state than for hydrolysis. In a comparison model, a test TS structure was generated, which incorporated the incoming imidazole nucleophile at 0.18 bond order (1.99 Å) and the leaving nicotinamide group at 0.025 bond order (2.58 Å). The predicted [1′-^{15}N] and [1′-^{14}C] KIEs are within 90% of the intrinsic KIE. The predicted [2′-^{3}H] KIE exhibited a 50% increase as compared to the intrinsic KIE. The predicted [1′-^{3}H] KIE was 1.029 for the transition state, far outside the experimental range of 1.194 ± 0.003. This calculation supports the proposed bond order assignments for the incoming and leaving groups. Bond lengths and bond orders for the reactant NAD$^+$ and transition state for NAD$^+$ hydrolysis and ADP ribosylation are summarized in Table 4, and the results for the analysis are provided for the reactants and transition states in Figure 6.

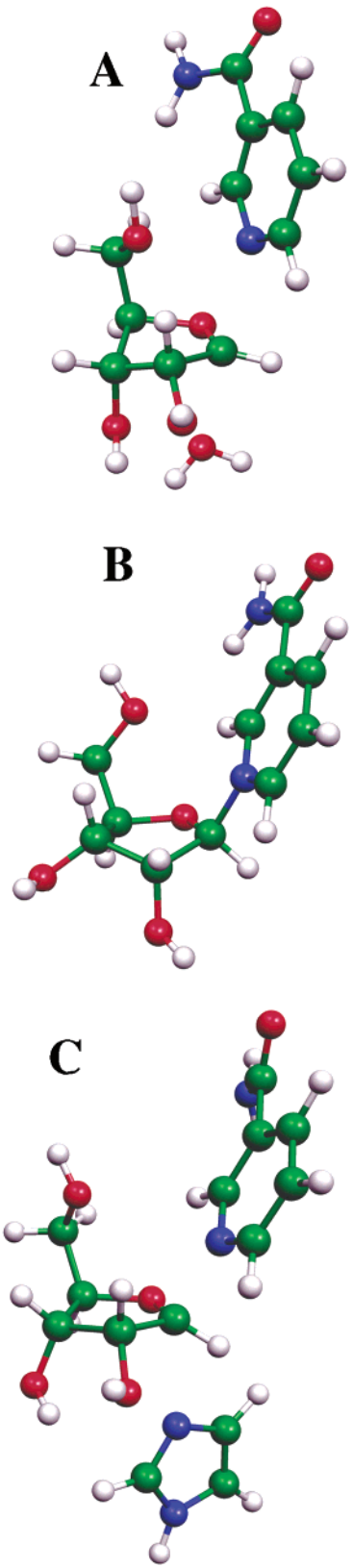

FIGURE 6: Transition state structure catalyzed by diphtheria toxin. (A) The transition state structure for NAD^+ hydrolysis of diphtheria toxin showing the nicotinamide riboside with the attacking water molecule. (B) Reactant state portion used from the X-ray crystal structure of NAD^+ bound to diphtheria toxin. (C) The transition state for the ADP ribosylation of eEF-2 by diphtheria toxin showing the nicotinamide riboside with the weak nucleophilic participation of the imidazole ring.

In contrast to DTA, the early transition state observed for pertussis toxin in the presence of G-protein is due to increased participation of the cysteine anion nucleophile (0.03 for hydrolysis and 0.11 for ADP ribosylation) (*22*, *29*, *37*). The ternary complex of DTA·NAD^+·eEF-2 reaches an early transition state by activation of the leaving group or increased oxacarbenium ion stabilization with no additional nucleophilic participation from the diphthamide. The relatively low nucleophilicity seen at the transition state is consistent with steric crowding from the bulky diphthamide nucleophile. However, eEF-2 binding activates transition state formation to increase the reaction rate by 1700-fold. This pattern of *N*-ribosyl transfer is possible in reactions that conform to nucleophilic displacement by electrophile migration (*38*−*40*). However, in this case, the presence of eEF-2 must stabilize the ribooxacarbenium ion and/or activate the leaving group without adding nucleophilic participation. The participation of active site residue, Glu148, has been proposed to stabilize the transition state for the glycohydrolase and ADP ribosyltransferase reactions, thereby assisting in formation of the transition state well before the formation of the fully developed oxacarbenium ion (*26*, *41*).

The crystal structure for the complex of DTA and NAD^+ shows the Glu148 carboxylate 4.5 ± 0.5 Å from C1′ of bound NAD^+. Molecular dynamics analysis of the complex does not suggest greatly improved interactions when investigating the transition state for NAD^+ hydrolysis (*42*). There are no structures of NAD^+ (or NAD^+ analogues) in complex with eEF-2 at the catalytic site of DTA. These complexes are expected to exhibit conformational changes, and on the basis of the present results, it would be predicted that Glu148 would be in a more favorable position to stabilize the early transition state structure observed from isotope effect analysis.

CONCLUSIONS AND SPECULATIONS

The transition state structure for ADP ribosylation by diphtheria toxin reveals early formation of the transition state with only weak nucleophilic participation by the diphthamide nitrogen of eEF2. Stabilization of the transition state ribooxacarbenium ion by Glu148 or activation of the nicotinamide group by a decreased dielectric of the leaving group pocket could be responsible. Although transition state analysis provides a two-state comparison of reactant and transition state, we can speculate on the atomic changes that follow transition state formation. In at least three other *N*-ribosyl transferases, the transition states are similar to that seen here, with 0.1−0.3 bond order remaining to the leaving group but only a few percent bond order to the attacking nucleophile. The reaction coordinate is established by enzymatic immobilization of leaving group and attacking nucleophile. The ribooxacarbenium ion is generated by catalytic site interactions, and C1′ migrates 1.8−2.1 Å from the leaving group to nucleophile. This reaction mechanism is called "nucleophilic displacement by electrophile migration" (*38*−*40*). All of the results reported here are consistent with, but do not prove, this mechanism. If ADP ribosylation of eEF-2 conforms to this mechanism, the transition state is reached after the ribosyl C1′ translates only 0.45 Å from immobilized nicotinamide toward the bound diphthamide. At the transition state, C1′ is still 2.58 Å from the diphthamide nucleophile, requiring a further excursion of approximately 1.1 Å to complete the reaction coordinate and product formation. In this mechanism, the nucleophile is activated by the catalytic

site environment but is not coupled to leaving group departure except in the sense that migration of the ribosyl group from nicotinamide brings it closer to the diphthamide nucleophile. It should be noted that this mechanism permits wide variation of pK_a values between leaving group and nucleophile, giving rise to asymmetric transition states and permitting reaction of the reactive oxacarbenium ion with a range of nucleophiles. For NAD^+-based ADP ribosyl transferases, the nucleophile diversity includes water, Arg, Cys, diphthamide, N1 of adenosine (in CD38), and carbonyl oxygens (in SIR2).

Transition state analogues that incorporate the 1,4-dideoxy-4-aminoiminoribitol group are powerful inhibitors at the nanomolar to picomolar range for nucleoside hydrolases and phosphorylases (*43*, *44*). Although ADP-ribosylating toxins, phosphorylases, and nucleoside hydrolases all proceed through ribooxacarbenium ion transition states, transition state analogue affinities are likely to be reduced for the ADP-ribosylating toxins because of the relatively small k_{enz}/k_{chem} ratio. In the later cases, rate enhancements are estimated to be 10^{12}, while for NAD^+ hydrolysis and ADP ribosylation, enhancements are 10^6-10^9. Although transition state analysis provides us with novel insight to catalysis, these poor catalysts may resist our efforts to design tight-binding transition state analogues.

ACKNOWLEDGMENT

We are grateful to Professor John Collier at Harvard Medical School for the gift of DTA expression plasmid. We thank Professor Hong Zhang from the University of Texas Southwestern Medical Center for proving the expression plasmid for NAD^+ pyrophosphorylase and Dr. Konstantin Shatalin at Intergrated Genomics Inc. for providing purified NAD^+ synthetase. Supported by NIH Grant AI34342.

REFERENCES

1. Domenighini, M., Pizza, M., and Rappuoli, R. (1995) *Bacterial Toxins and Virulence Factors in Disease*, Marcel Dekker, Inc., New York, Basel, Hong Kong.
2. Althaus, F. R., and Richter, C. (1987) ADP-ribosylation of proteins. Enzymology and biological significance, *Mol. Biol. Biochem. Biophys. 37*, 1−237.
3. Locht, C., and Antoine, R. (1997) *Bacterial Toxins: Tools in Cell Biology and Pharmacology*, Chapman & Hall, Weinheim, Germany.
4. Van den Akker, F., Merritt, E. A., and Hol, W. G. J. (2000) *Bacterial Protein Toxins*, Springer, Berlin.
5. Van Ness, B. G., Howard, J. B., and Bodley, J. W. (1980) ADP-ribosylation of elongation factor 2 by diphtheria toxin. NMR spectra and proposed structures of ribosyl-diphthamide and its hydrolysis products, *J. Biol. Chem. 255*, 10710−10716.
6. Schiavo, G., Rossetto, O., and Montecucco, C. (1994) Clostridial neurotoxins as tools to investigate the molecular events of neurotransmitter release, *Semin. Cell. Biol. 5*, 221−229.
7. Moldave, K. (1985) Eukaryotic protein synthesis, *Annu. Rev. Biochem. 54*, 1109−1149.
8. Mattheakis, L. C., Sor, F., and Collier, R. J. (1993) Diphthamide synthesis in *Saccharomyces cerevisiae*: structure of the DPH2 gene, *Gene 132*, 149−154.
9. Schultz, D. C., Balasara, B. R., Testa, J. R., and Godwin, A. K. (1998) Cloning and localization of a human diphthamide biosynthesis-like protein-2 gene, DPH2L2, *Genomics 52*, 186−191.
10. Chung, D. W., and Collier, R. J. (1977) The mechanism of ADP-ribosylation of elongation factor 2 catalyzed by fragment A from diphtheria toxin, *Biochim. Biophys. Acta 483*, 248−257.
11. Gill, D. M., Pappenheimer, A. M., Jr., Brown, R., and Kurnick, J. T. (1969) Studies on the mode of action of diphtheria toxin. VII. Toxin-stimulated hydrolysis of nicotinamide adenine dinucleotide in mammalian cell extracts, *J. Exp. Med. 129*, 1−21.
12. Scheuring, J., and Schramm, V. L. (1995) Stereochemistry of the ADP-Ribosylation Catalyzed by Pertussis Toxin, *J. Am. Chem. Soc. 117*, 12653−12654.
13. Oppenheimer, N. J., and Bodley, J. W. (1981) Diphtheria toxin. Site and configuration of ADP-ribosylation of diphthamide in elongation factor 2, *J. Biol. Chem. 256*, 8579−8581.
14. Oppenheimer, N. J. (1978) Structural determination and stereospecificity of the choleragen-catalyzed reaction of NAD^+ with guanidines, *J. Biol. Chem. 253*, 4907−4910.
15. Rising, K. A., and Schramm, V. L. (1994) Enzymic Synthesis of NAD^+ with the Specific Incorporation of Atomic Labels, *J. Am. Chem. Soc. 116*, 6531−6536.
16. Zhang, X., Kurnasov, O. V., Karthikeyan, S., Grishin, N. V., Osterman, A. L., and Zhang, H. (2003) Structural characterization of a human cytosolic NMN/NaMN adenylyltransferase and implication in human NAD biosynthesis, *J. Biol. Chem. 278*, 13503−13511.
17. Wilson, B. A., Reich, K. A., Weinstein, B. R., and Collier, R. J. (1990) Active-site mutations of diphtheria toxin: effects of replacing glutamic acid-148 with aspartic acid, glutamine, or serine, *Biochemistry 29*, 8643−8651.
18. Jorgensen, R., Carr-Schmid, A., Ortiz, P. A., Kinzy, T. G., and Andersen, G. R. (2002) Purification and crystallization of the yeast elongation factor eEF2, *Acta Crystallogr. D: Biol. Crystallogr. 58*, 712−715.
19. Bradford, M. M. (1976) A rapid and sensitive method for the quantitation of microgram quantities of protein utilizing the principle of protein-dye binding, *Anal. Biochem. 72*, 248−254.
20. Rose, I. (1980) The isotope trapping method: desorption rates of productive E.S complexes, *Methods Enzymol. 64*, 47−59.
21. Rose, I. (1995) Partition Analysis: Detecting Enzyme Reaction Cycle Intermediates, *Methods Enzymol. 249*, 315−340.
22. Scheuring, J., Berti, P. J., and Schramm, V. L. (1998) Transition-state structure for the ADP-ribosylation of recombinant Gialpha1 subunits by pertussis toxin, *Biochemistry 37*, 2748−2758.
23. Frisch, M. J. T., Schlegel, H. B., Scuseria G. E., Robb, M. A., Cheeseman, J. R., Zakrzewski, V. G., Montgomery, J. A., Jr., Stratmann, R. E., Burant, J. C., Dapprich, S., Millam, J. M., Daniels, A. D., Kudin, K. N., Strain, M. C., Farkas, O., Tomasi, J., Barone, V., Cossi, M., Cammi, R., Mennucci, B., Pomelli, C., Adamo, C., Clifford, S., Ochterski, J., Petersson, G. A., Ayala, P. Y., Cui, Q., Morokuma, K., Malick, D. K., Rabuck, A. D., Raghavachari, K., Foresman, J. B., Cioslowski, J., Ortiz, J. V., Stefanov, B. B., Liu, G., Liashenko, A., Piskorz, P., Komaromi, I., Gomperts, R., Martin, R. L., Fox, D. J., Keith, T., Al-Laham, M. A., Peng, C. Y., Nanayakkara, A., Gonzalez, C., Challacombe, M., Gill, P. M. W., Johnson, B., Chen, W., Wong, M. W., Andres, J. L., Gonzalez, C., Head-Gordon, M., Replogle, E. S., Pople, J. A. (1998) Gaussian Inc., Pittsburgh, PA.
24. Bell, C. E., and Eisenberg, D. (1996) Crystal structure of diphtheria toxin bound to nicotinamide adenine dinucleotide., *Biochemistry 35*, 1137−1149.
25. Anisimov, V., and Paneth, P. (1999) ISOEFF98. A program for studies of isotope effects using Hessian modifications, *J. Math. Chem. 26*, 75−86.
26. Berti, P. J., Blanke, S. R., and Schramm, V. L. (1997) Transition State Structure for the Hydrolysis of NAD^+ Catalyzed by Diphtheria Toxin, *J. Am. Chem. Soc. 119*, 12079−12088.
27. Blanke, S. R., Huang, K., and Collier, R. J. (1994) Active-site mutations of diphtheria toxin: role of tyrosine-65 in NAD binding and ADP-ribosylation, *Biochemistry 33*, 15494−15500.
28. Dolan, K. M., Lindenmayer, G., and Olson, J. C. (2000) Functional comparison of the NAD binding cleft of ADP-ribosylating toxins, *Biochemistry 39*, 8266−8275.
29. Scheuring, J., and Schramm, V. L. (1997) Pertussis toxin: transition state analysis for ADP-ribosylation of G-protein peptide alphai3C20, *Biochemistry 36*, 8215−8223.
30. Northrop, D. B. (1981) The expression of isotope effects on enzyme-catalyzed reactions, *Annu. Rev. Biochem. 50*, 103−131.
31. Chen, X. Y., Link, T. M., and Schramm, V. L. (1998) Ricin A-chain: kinetics, mechanism, and RNA stem-loop inhibitors, *Biochemistry 37*, 11605−11613.
32. Schramm, V. L. (1997) Enzymatic N-riboside scission in RNA and RNA precursors, *Curr. Opin. Chem. Biol. 1*, 323−331.
33. Berti, P., and Schramm, V. (1997) Transition State Structure of the Solvolytic Hydrolysis of NAD^+, *J. Am. Chem. Soc. 119*, 12069−12078.
34. Mentch, F., Parkin, D. W., and Schramm, V. L. (1987) Transition-state structures for N-glycoside hydrolysis of AMP by acid and

by AMP nucleosidase in the presence and absence of allosteric activator, *Biochemistry 26*, 921−930.
35. Scheuring, J., and Schramm, V. L. (1997) Kinetic isotope effect characterization of the transition state for oxidized nicotinamide adenine dinucleotide hydrolysis by pertussis toxin, *Biochemistry 36*, 4526−4534.
36. Rising, K. A., and Schramm, V. L. (1997) Transition State Analysis of NAD^+ Hydrolysis by the Cholera Toxin Catalytic Subunit, *J. Am. Chem. Soc. 119*, 27−37.
37. Berti, P. J., and Tanaka, K. E. (2002) Transition State Analysis Using Multiple Kinetic Isotope Effects: Mechanisms of Enzymatic and Nonenzymatic Glycoside Hydrolysis and Transfer, *Adv. Phys. Org. Chem. 37*, 239−314.
38. Schramm, V. L., and Shi, W. (2001) Atomic motion in enzymatic reaction coordinates, *Curr. Opin. Struct. Biol. 11*, 657−665.
39. Shi, W., Tanaka, K. S., Crother, T. R., Taylor, M. W., Almo, S. C., and Schramm, V. L. (2001) Structural Analysis of Adenine Phosphoribosyltransferase from *Saccharomyces cerevisiae*, *Biochemistry 40*, 10800−10809.
40. Fedorov, A., Shi, W., Kicska, G., Fedorov, E., Tyler, P. C., Furneaux, R. H., Hanson, J. C., Gainsford, G. J., Larese, J. Z., Schramm, V. L., and Almo, S. C. (2001) Transition state structure of purine nucleoside phosphorylase and principles of atomic motion in enzymatic catalysis, *Biochemistry 40*, 853−860.
41. Bell, C. E., and Eisenberg, D. (1997) Crystal structure of diphtheria toxin bound to nicotinamide adenine dinucleotide, *Adv. Exp. Med. Biol. 419*, 35−43.
42. Kahn, K., and Bruice, T. C. (2001) Diphtheria toxin catalyzed hydrolysis of NAD(+): molecular dynamics study of enzyme-bound substrate, transition state, and inhibitor, *J. Am. Chem. Soc. 123*, 11960−11969.
43. Miles, R. W., Tyler, P. C., Evans, G. B., Furneaux, R. H., Parkin, D. W., and Schramm, V. L. (1999) Iminoribitol transition state analogue inhibitors of protozoan nucleoside hydrolases, *Biochemistry 38*, 13147−13154.
44. Miles, R. W., Tyler, P. C., Furneaux, R. H., Bagdassarian, C. K., and Schramm, V. L. (1998) One-third-the-sites transition-state inhibitors for purine nucleoside phosphorylase, *Biochemistry 37*, 8615−8621.

BI035907Z